

## **Influence of Precipitate Morphology on Hardness and Electrical Conductivity of Heat-treatable Aluminum Alloys**

Shengping Yuan<sup>1</sup>, Gang Liu<sup>1</sup>, Ruihong. Wang<sup>1</sup>, Guojun Zhang<sup>1</sup>, Xiong. Pu<sup>1</sup>, Jun. Sun<sup>1</sup> and Kanghua Chen<sup>2</sup>

<sup>1</sup>State Key Laboratory for Mechanical Behavior of Materials, School of Materials Science & Engineering, Xi'an Jiaotong University, Xi'an, 710049, China

<sup>2</sup>State Key Laboratory for Powder Metallurgy, The University of Southern Central China, Changsha, 410083, China

Because of the complex composition and complicated thermal-mechanical treatment, precipitates in heat-treatable aluminum alloys usually have diverse morphology. How the macro properties depend on the precipitate morphology has not been well known. In this paper, a two-step aging treatment has been employed to an aged Al-Mg-Si alloy to develop the evolution of precipitate morphology, from spherical gradually to predominantly rod- and needle-shaped. Experimental and calculation results show that the hardening effect of spherical precipitates dominates over the precipitation hardening rather than that of rod-/needle-shaped precipitates, because the dislocations interaction with spherical precipitates is stronger than that with rod-/needle-shaped precipitates. On the contrary, the electrical conductivity is found to be most sensitive to rod- or needle-shaped precipitates that could form an effective barrier net to hinder the mass migration. All calculated results are in good agreement with experimental observations.

**Keywords:** *precipitate morphology, Al-Mg-Si alloy, precipitation hardening, electrical conductivity.*

### **1. Introduction**

In heat-treatable aluminum alloys, the resulting mechanical properties, especially hardness or yield strength, are directly related to the volume fraction and size of precipitates which form during artificial aging treatment [1-3]. In the underaged stage until to peak-aged condition, the increasing volume fraction and size causes a successive enhancement in hardness. In the overaged stage, where precipitates coarsen via Ostwald ripening, hardness goes down. Besides, precipitate morphology evolution can also affect hardness during aging treatment. However, there have been few work reported to study the influence of precipitate morphology on hardening effect. The present paper will be firstly focused on this issue.

The second focus in the present paper is how the precipitate morphology can influence the electrical conductivity. Besides mechanical properties, electrical properties are also of key interest to the industrial manufacture and application of the heat-treatable aluminum alloys. The electrical resistance measurements are a much sensitive tool for studying the precipitation in Al-Mg-Si alloys [4-6], and have become an effective non-destructive technique for monitoring the aging response. Several models [7-9] have been suggested to relate the aging dependent electrical properties to the precipitate evolutions, all based on the experiment where a single type of precipitates existed. There have been limited understandings on the effect of multiple precipitates or the precipitate morphology evolution on the electrical conductivity .

In this paper, a two-step aging treatment has been employed to an Al-Mg-Si alloy to obtain the evolution of precipitate morphology, from spherical to predominantly rod- and needle-shaped, which can help us to understand the relationship between precipitate morphology and hardness and electrical conductivity.

## 2. Experimental procedures

The Al-Mg-Si alloys used in present investigation are extruded rods of 18 mm in diameter. The composition in weight percentage is 1.12 % Mg, 0.57 % Si, 0.25 % Cu, 0.22 % Cr, and balance Al. The alloys had been solution-treated at 703 K for half-hour followed by water quench and then been pre-aged at 373 K for 20 minutes. After stored at room temperature for 50 months, the alloys were secondly aged for a series of time from 2 h to 40 h at 473 K and 523K, respectively.

Hardness measurements were performed using the Vickers microhardness technique by measuring the averages of at least 10 indentations each at several locations on each sample. The applied load was 5 kg and holding time was 30 s. Electrical conductivity was measured by using a 7501 conductivity meter with a 12.7 mm (0.5 in.) probe. At least three measurements were performed on different locations of the test samples. In microstructural analyses, transmission electron microscope (TEM) was used to determine the size and volume fraction of the precipitates. Details could be referred to our previous paper [10-12].

## 3. Experimental results

### 3.1 Evolution of precipitate morphology

Fig. 1 (a) shows the microstructure image of the sample before secondary aging treatment, where the spherical precipitates, determined as metastable pre- $\beta''$  phase of  $\text{AlMg}_4\text{Si}_6$  [12], were precipitated during the first aging treatment and subsequently grow during the following storage period. In the secondary aging treatment, it was found that the spherical pre- $\beta''$  precipitates decrease gradually. On the other hand, two other kinds of hardening second phase particles were being precipitated, which are rod-shaped precipitates and needle-shaped precipitates, respectively, as typically shown in Fig. 1 (b). The rod-shaped precipitates, determined as metastable  $\beta''$  phase of  $\text{Mg}_5\text{Si}_6$ , formed *in situ* on the pre- $\beta''$  phase and grew by consuming the pre- $\beta''$  phase, while the needle-shaped precipitates, determined as metastable  $\beta'$  phase of  $\text{Mg}_2\text{Si}$ , were precipitated from the matrix. Details about variation of volume fraction and size of multiple precipitates during aging treatment can be found in our previous paper, which will be used for subsequent calculations in next section.

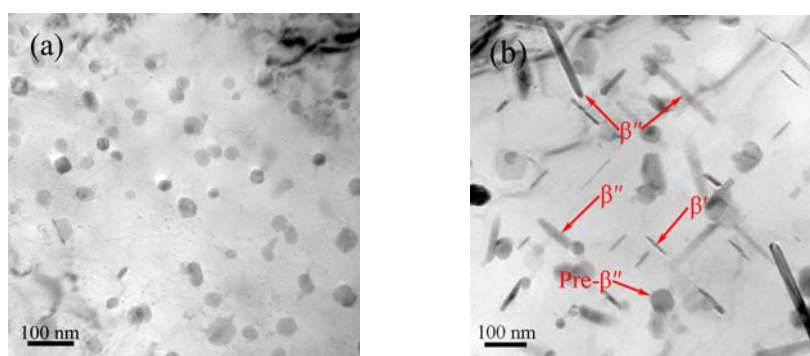


Fig. 1 Typical TEM images showing the morphology and size of pre- $\beta''$  precipitates of  $\text{AlMg}_4\text{Si}_6$  before secondary aging treatment (a) and of multiple precipitates, i.e., sphere-shaped pre- $\beta''$  particles of  $\text{AlMg}_4\text{Si}_6$ , rod-shaped  $\beta''$  precipitates of  $\text{Mg}_5\text{Si}_6$ , and needle-shaped  $\beta'$  precipitates of  $\text{Mg}_2\text{Si}$ , after secondary aging treatment.

### 3.2 Mechanical and electrical properties

Corresponding to the variation of multiple precipitates during aging treatment, the sample exhibited a remarkable change in mechanical and electrical properties. Table 1 summarizes the measured hardness and electrical conductivity of the Al-Mg-Si alloys. It is surprisingly found that the hardness decreases gradually in the secondary aging treatment. This unusual result may be associated with the much long storage at room temperature before the secondary aging treatment. During the storage, the pre- $\beta''$  particles that nucleated in the pre-aging treatment grew up to effective hardening

obstacles and had intense hardening effect. In comparison, the rod-shaped  $\beta''$  particles and the needle-shaped  $\beta'$  particles precipitated during the secondary aging treatment have less hardening effect. As a result, the decrease in volume fraction of the pre- $\beta''$  particles during the secondary aging treatment caused the reduction in hardness. One can also find from Table 1 that electrical conductivity increases with aging time, which will be discussed in next section.

Table 1 Measurements on hardness and electrical conductivity

$t$ (h)	$T$ (K)/ $Hv$		$T$ (K)/ $\kappa$ ( $10^6 \Omega^{-1}m^{-1}$ )	
	473	523	473	523
0	102( $\pm 4$ )	102( $\pm 4$ )	18.2( $\pm 0.6$ )	18.2( $\pm 0.5$ )
2	90( $\pm 3$ )	85( $\pm 2$ )	19.5( $\pm 0.6$ )	19.0( $\pm 1.2$ )
5	87( $\pm 4$ )	82( $\pm 3$ )	20.5( $\pm 0.6$ )	20.2( $\pm 1.2$ )
10	85( $\pm 3$ )	79( $\pm 2$ )	22.0( $\pm 0.6$ )	19.9( $\pm 0.5$ )
20	82( $\pm 4$ )	76( $\pm 4$ )	22.9( $\pm 1.1$ )	19.6( $\pm 0.6$ )
40	80( $\pm 2$ )	73( $\pm 2$ )	23.6( $\pm 1.2$ )	20.0( $\pm 1.1$ )

## 4. Discussion

### 4.1 Effect of precipitate morphology on hardening

The hardening effect in heat-treatable aluminum alloys mainly comes from precipitates. It has been well known that raising the precipitate content and reducing the precipitate size can promote the hardening effect. Besides, computer simulations have also revealed that precipitates with different shapes should have different hardening response [13]. When the precipitates are unsharable, the increment in yield strength caused by spherical precipitates ( $\Delta\sigma_s$ ) can be expressed as [3]

$$\Delta\sigma_s = \frac{M}{r_s} (2\psi Gb) \left( \frac{3f_s}{2\pi} \right)^{1/2} \quad (1)$$

where  $M$  is the Taylor factor ( $\sim 3.1$ ),  $G$  is the shear modulus (28 GPa [14]),  $b$  is the magnitude of Burgers vector in Al (0.286 nm [14]),  $\psi$  is a constant close to 0.5, and  $r_s$  (about 15 nm) and  $f_s$  are mean particle size and volume fraction of the spherical precipitates, respectively. On the other hand, the increment in yield strength caused by rod- and/or needle-shaped precipitates ( $\Delta\sigma_{r/n}$ ) is [15]

$$\Delta\sigma_{r/n} = 0.065 M G \frac{b}{\sqrt{r_{r/n} l_{r/n}}} \left[ f_{r/n}^{1/2} + 0.75 \left( \frac{r_{r/n}}{l_{r/n}} \right)^{1/2} f + 0.14 \left( \frac{r_{r/n}}{l_{r/n}} \right) f^{3/2} \right] \ln \left( \frac{0.158 r_{r/n}}{r_0} \right) \quad (2)$$

where subscript  $r/n$  means the expression is either for the rod-shaped  $\beta''$  precipitates or for the needle-shaped  $\beta'$  precipitates, and  $r_0$  denotes the inner cut-off radius (0.572 nm) for calculation of the dislocation line tension. The ratio between  $\Delta\sigma_s$  and  $\Delta\sigma_{r/n}$  ( $\Delta\sigma_s / \Delta\sigma_{r/n}$ ) can be used to simply estimate the difference in hardening effect between spherical and rod-/needle-shaped precipitates. At a volume fraction of  $f_s = f_{r/n} = 0.8\%$  that corresponds approximately to the decrease in  $f_s$  and concomitant increase in the sum of  $f_r$  and  $f_n$  during the aging treatment,  $\Delta\sigma_s / \Delta\sigma_{r/n}$  is calculated as a function of the aspect ratio ( $l_{r/n} / r_{r/n}$ ) of the rod-/needle-shaped precipitates, as shown in Fig. 2 (a). The spherical precipitates are clearly found to have a hardening effect superior to the rod-/needle-shaped precipitates (in present alloys,  $r_r$  is about  $1/3 \sim 1/4 r_s$  and  $l_{r/n} / r_{r/n}$  is about  $7 \sim 15$ ). This indicates that the dislocations interaction with the spherical precipitates is stronger than that with the rod-/needle-shaped precipitates, which is responsible for the decrease in yield strength with

precipitate morphology evolution in present experiments. The dislocation interaction is related to the precipitate interface and local strain field around the precipitates. The rod-/needle-shaped precipitates have well-ordered interface along the long axial direction, while the spherical precipitate have a much small fraction of this well-ordered interface. The local strain field around spherical precipitates is more intense than that around rod-/needle-shaped precipitates. This yields a stronger interaction between dislocation and the spherical precipitates. In Fig. 2 (b), one can find that dislocations are pinned mostly by spherical precipitates rather than by rod-shaped precipitates.

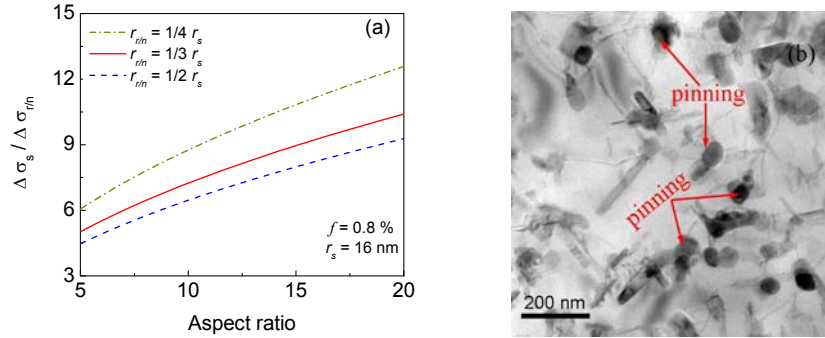


Fig. 2 (a) Dependence of  $\Delta\sigma_s / \Delta\sigma_{r/d}$  on rod-/needle-shaped precipitate size ( $r_{r/d}$ ) as a function of the aspect ratio of the rod-/needle-shaped precipitates; (b) Typical TEM image showing the pinning of dislocations by spherical precipitates.

#### 4.2 Effect of precipitate morphology on electrical conductivity

Most recently, Raeisnia et al.'s experiments [4] showed that the contribution of the precipitates to the overall electrical resistivity was inversely proportional to the square root of the interparticle spacing of the precipitates. This conclusion will be employed here to model the aging dependent electrical conductivity of Al-Mg-Si alloys.

For simplicity, the electrical resistivity ( $\rho$ ) will be firstly modeled and subsequently turn into the electrical conductivity,  $\kappa$  ( $= 1/\rho$ ). According to Raeisnia et al. [4], a more general form of Matthiessen's law by including an extra term to account for the effect of precipitates on resistivity

( $\rho_p = \frac{D}{\lambda_p^{1/2}}$ ) is as

$$\rho = \rho_M + \sum_i \rho_i C_i + \frac{D}{\lambda_p^{1/2}}. \quad (3)$$

where  $\rho_M$  is the resistivity of pure Al at the measurement temperature,  $\sum_i \rho_i C_i$  the summation of the resistivity contributions from the various solid solution contributions ( $\rho_i$  is the specific resistivity of the  $i$ -th solute and  $C_i$  is the concentration of this solute,  $i$  represents Mg, Si and Cu in present model), and  $D$  is a constant calibrated from experimental results. Because present Al-Mg-Si alloys contain multiple precipitates, three cases will be also considered. Correspondingly, Eq. 3 could be rewritten into three different versions as follows.

Case I (considering a single kind of precipitates):

$$\rho = \rho_M + \sum_i \rho_i C_i + \frac{D}{\lambda_i^{1/2}}, \quad i = s, \text{ or } r, \text{ or } n. \quad (4)$$

Case II (considering three kinds of precipitates but independent of density):

$$\rho = \rho_M + \sum_i \rho_i C_i + \frac{3D}{\sum_i \lambda_i^{1/2}}, \quad i = s, r, \text{ and } n. \quad (5)$$

Case III (considering three kinds of precipitates and density-dependent)

$$\rho = \rho_M + \sum_i \rho_i C_i + \frac{D}{\sum_i (n_i \lambda_i^{1/2})}, \quad i = s, r, \text{ and } n. \quad (6)$$

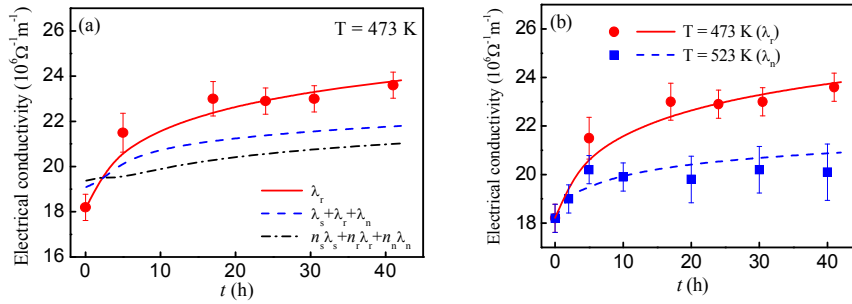


Fig. 3 Experimental and calculated dependence of the electrical conductivity ( $\kappa$ ) on  $t$  at  $T = 473$  K and  $523$  K. Dots are experimental results and lines are calculations. In (a), calculations are based on Case I (Eq. 4), Case II (Eq. 5), and Case III (Eq. 6). Calculations fitting well with the experiments at both the two aging temperature are summarized in (b).

Calculations show that neither Eq. 5 nor Eq. 6 can satisfactorily describe the experimental evolution of electrical conductivity with aging temperature and aging time, as typically depicted in Fig. 3 (a) as dash line and dash-dot line, respectively. When Eq. 4 is used, however, calculations match well with the experiments (see Fig. 3(b), input data for calculation are  $\rho_{Mg} = 4$  n $\Omega$  m/at%,  $\rho_{Si} = 6$  n $\Omega$  m/at%,  $\rho_{Cu} = 10$  n $\Omega$  m/at%, and  $D = 320$  n $\Omega$  m $\cdot$ nm $^{1/2}$ , respectively.) by considering only the  $r$  particles (rod-shaped  $\beta''$  precipitates) at  $473$  K and the  $n$  particles (needle-shaped  $\beta'$  precipitates) at  $523$  K, respectively. This indicates that the present alloy, although containing three kinds of precipitates, should exhibit electrical conductivity most sensitive to only a single kind of precipitates that have the most dominant hindrance effect to conduction electron flux. Because longer particles have more intense hindrance effect, the rod-shaped  $\beta''$  precipitates and the needle-shaped  $\beta'$  precipitates should be most possible to become the dominant ones. At  $473$  K, the growth of the  $\beta'$  precipitates is somewhat limited and so the much longer  $\beta''$  precipitates become the dominant barrier to the mass migration (Fig. 4 (a)). While at  $523$  K, further growth of the  $\beta''$  precipitates makes the interparticle spacing too far to form an effective barrier net. On the other hand, the grown  $\beta'$  precipitates that distributed between the  $\beta''$  precipitates will replace the  $\beta''$  precipitates to become the dominant barrier (Fig. 4 (b)).

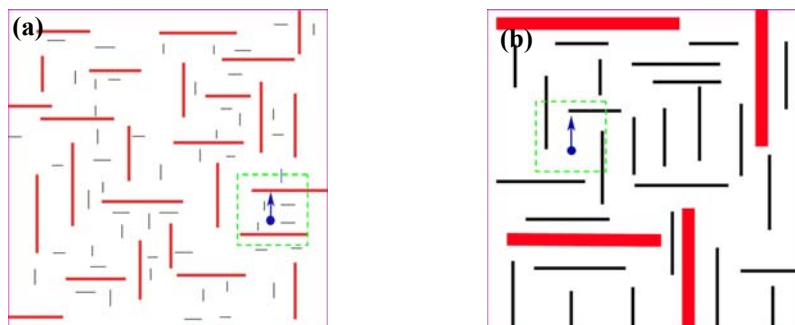


Fig. 4 Sketches illustrating the rod-shaped  $\beta''$  and needle-shaped  $\beta'$  precipitates forming the dominant effective hindrance net to mass migration in (a)  $T = 473$  K, and (b)  $T = 523$  K, respectively.

Finally, it should be addressed that the dependence of electrical properties on the multiple precipitates may be much complicated because the scattering effect of any precipitates should contribute to the resistivity. Besides, if an effective interparticle spacing averaging over the three kinds of precipitates could be obtained by using more advanced technique, the electrical properties may be directly related to the effective interparticle spacing with more precision. The crude results presented in this paper provide only a phenomenological relationship between the electrical conductivity and the geometrical distribution of precipitates, which, however, once combining with the results on hardness, should be also very helpful for the artificial controlling precipitate morphology and so for the theory-aided design of alloys to achieve superior combination of mechanical properties and electrical properties.

## 5. Conclusions

(1) The precipitate morphology evolution in an Al-Mg-Si alloy, from full spherical to predominant rod-/needle-like, causes decrease in hardness, which indicates that the hardening effect of spherical precipitates is larger than that of rod-/needle-shaped precipitates, because the dislocations interaction with spherical precipitates is stronger than that with rod-/needle-shaped precipitates.

(2) Although containing three kinds of precipitates, the alloy exhibits electrical conductivity most sensitive to a dominant kind of precipitates, i.e., rod-shaped  $\beta''$  precipitates at 473 K and needle-shaped  $\beta'$  precipitates at 523 K, respectively. This is because the two kinds of precipitates can form an effective barrier net to hinder the mass migration. The influence of precipitate morphology on the mechanical properties is much different from that on the electrical properties.

## 6. Acknowledgments

This work was supported by the National Basic Research Program of China (Grant No. 2010CB631003 & 2005CB623700) and the National Natural Science Foundation (50701035). This work was also supported by the 111 Project of China under Grant No. B06025.

## References

- [1] E. Hornbogen and E. A. Starke Jr: *Acta Metall.* 41 (1993) 1-16.
- [2] H. R. Shercliff and M. F. Ashby: *Acta Metall.* 38 (1990) 1789-1802
- [3] O. R. Myhr, Ø. Grong and S. J. Andersen: *Acta Mater.* 49 (2001) 65-75.
- [4] B. Raeesinia, W. J. Poole and D. J. Lloyd: *Mater Sci Eng A.* 420 (2006) 245-249.
- [5] M. A. Gaffar, A. Gaber and M. S. Mostafa and E. F. Abo Zeid: *Mater Sci Eng A.* 465 (2007) 274-282.
- [6] L. Lodgaard and N. Ryum: *Mater Sci Eng A.* 283 (2000) 144-152.
- [7] P. Guyot P and L. Cottignies: *Acta Mater.* 44 (1996) 4161-4167.
- [8] M. J. Starink and X. M. Li: *Metall Trans A.* 34 (2002) 899-911.
- [9] R. C. Dorward: *Mater Sci Tech.* 15 (1999) 1133-1138.
- [10] S. P. Yuan, G. Liu, R. H. Wang, X. Pu, G. J. Zhang, J. Sun and K. H. Chen KH: *Scripta Mater.* 57 (2007) 865-868.
- [11] S. P. Yuan, G. Liu, R. H. Wang, G. J. Zhang, X. Pu, J. Sun and K. H. Chen KH: *Scripta Mater.* 60 (2009) 1109-1112.
- [12] S. P. Yuan, G. Liu, R. H. Wang, G. J. Zhang, X. Pu, J. Sun and K. H. Chen KH: *Scripta Mater.* 499 (2009) 387-395.
- [13] J. F. Nie: *Scripta Mater.* 48 (2003) 1009-1015.
- [14] G. Liu, G. J. Zhang, X. D. Ding, J. Sun, K. H. Chen: *Mater Sci Eng A.* 344 (2003) 113-124.

[15] A. W. Zhu and E. A. Starke Jr: *Acta Mater* 47 (1999) 3263-3269.